Pharm Res (2014) 31:2463–2478
DOI 10.1007/s11095-014-1341-3

RESEARCH PAPER

Nanofiber-Coated Drug Eluting Stent for the Stabilization of Mast Cells

Byeongtaek Oh • Chi H. Lee

Received: 8 November 2013 / Accepted: 13 February 2014 / Published online: 25 March 2014

ABSTRACT

Purpose The nanofiber-hydrogel blend containing nitric oxide (NO) donors and reactive oxygen species (ROS) scavengers (Edaravone: EDV) was explored as an advanced strategy for stabilization of Mast cells (MCs) to achieve efficient immune-suppressive effects.

Methods Three types of nanofiber hydrogel composites (Bare-Nanofibers (BNF), Nanofiber-Hydrogels (NF-Gel) and Cross-linked Nanofiber-Hydrogels (NF-Gel-X)), were evaluated. The degranulation rates of MCs were determined by measurement of the extracellular levels of hydrogen peroxide and the released amounts of β-hexosaminidase from the activated-MCs (a-MCs). In addition, the effects of EDV on the selective scavenging of the oxygen radicals and prevention of peroxynitrite formation were evaluated. The roles of a-MCs in re-endothelialization and viability of coronary artery endothelial cells (hPCAECs) were defined using alamar blue and LDH assay, respectively.

Results Each polymer matrix has unique morphological characteristics. The effects of EDV (~1.0 mM) on the production of NO were greatly influenced by the presence of superoxide or hydroxyl radicals. NF-G-X containing a mixture of EDV and S-Nitroglutathione (GSNO) produced the highest level of NO under the oxidative stress conditions. GSNO alone or a mixture of GSNO and EDV significantly lowered the degranulation rate of a-MCs (GSNO only: 55.8 ± 5.4%; GSNO with EDV: 50.6 ± 0.6%), indicating that NO plays an integral role in degranulation of a-MCs. There were no significant biochemical evidences of cytotoxic effects of GSNO and EDV on the hPCAECs.

Conclusions Nanofibers containing a mixture of nitric oxide donors and ROS scavengers could be used as a promising strategy to stabilize MCs from the ROS-mediated immune responses.

B. Oh • C. H. Lee (✉)
Division of Pharmaceutical Sciences, School of Pharmacy
University of Missouri-Kansas City, 2464 Charlotte Street, HSB-4242
Kansas City, Missouri 64108, USA
e-mail: leech@umkc.edu

KEY WORDS Edaravone (EDV) · mast cells · nanofiber · nitric oxide (NO) · reactive oxygen species (ROS)

ABBREVIATIONS

a-MCs	Activated-Mast Cells
c48/80	Compound 48/80
EDV	Edaravone
GSNO	S-Nitroglutathione
RFUs	Relative fluorescent units

INTRODUCTION

An endovascular stent has been considered as one of the most important devices in the treatment of coronary artery diseases (CAD). There are numerous types of commercially available endovascular stents. They are bare-metal stent (BMS), polymeric-coated stent and drug-eluted stent (DES) (1). Despite considerable advancements and promising clinical outcomes, the recent studies reported that DES has triggered stent thrombosis in the late application stage and resulted in a long-term failure, especially after producing stenting complex lesions (2). This is due in part to the fact that anti-proliferative agents, such as Sirolimus and Paclitaxel, loaded in DES hindered smooth muscle cell (SMCs) migration as well as re-endothelialization of the substrate.

Various techniques, such as micro-pored film covering, biological membrane coating and endothelial progenitor cells (EPCs) seeding, have been introduced to improve surface morphology of DES and its therapeutic efficacy (3,4). Because the diameter and area of stent surface were very small, it is difficult to load and deliver a sufficient amount of drugs from DES for a longer period of time. In addition, as atheroma thin layer is exposed to luminal blood flow, the atheroma can be degraded by monocyte adhesion, that subsequently enhances the angioplasty inducible pressure. Recently, the stent coating

strategy with nanofiber has been emerged as an innovative breakthrough in interventional cardiology due to noticeable advantages; 1) it has a porous structure that could provide a large surface area for diffusion, rendering stents a desirable release profile, 2) the turbulent blood flow can be intervened with laminar flow, and 3) fibers can be designed to dissolve over an extended period of time to maintain the effective concentrations of loaded drugs for a desired duration (5,6).

Mast cells (MCs) play a critical role in allergic diseases, such as ventricular fibrosis, renal fibrosis and host defense (7,8). Antigen-mediated activation of MCs stimulated a subcellular-signaling cascade, that expelled secretory granules including cytokines, tryptase, chymase, hydrogen peroxide and histamine, resulting in promotion of allergic responses (9). Although the mechanisms behind the physiological role of MCs in cardiovascular diseases have not been fully elucidated, several studies have confirmed the essential role of MCs in cardiovascular diseases (10,11). A vast majority of physiological stimuli including reactive oxygen species (ROS) trigger the granular decomposition of MCs, potentially reversing the atheroprotective function into atherogenetic one (12). Therefore, the strategies intended to stabilize MCs will improve the immunosuppressive efficacy of coronary artery angioplasty *via* maintaining viability of coronary artery endothelial cells (hPCAECs) (10).

Reactive oxygen species (ROS) are considered as a harmful cause of various diseases including neurodegenerative disease, diabetes and cardiovascular disease (13). Under the physiological conditions, mitochondrial electron transport chain serves as the major source of ROS production (14). It was reported that the accumulation of ROS at the subcellular level disrupted the redox balance of endothelial cells, ultimately inducing cell apoptosis and triggering the rupture of atheroma thin layer (15). Under the hypoxic conditions, externally induced-ROS, such as oxidized-low density lipoprotein (ox-LDL) and hydrogen peroxide (H_2O_2), traversed through cellular membrane of activated-mast cells (a-MCs), subsequently disrupting ROS regulation and producing undesirable cell-signals including over-expression of MMP-2, -9 and NF-kB (16,17).

Nitric Oxide (NO) generated by endothelial nitric oxide synthase (eNOS) has been considered as a crucial protective molecule in the vasculature, that increases the blood flow, inhibits thrombus formation, regulates smooth muscle cells (SMCs) tone, and stimulates endothelial proliferation (15,18,19). Even though it is still unclear whether or not MCs derived from rat or human could generate endogenous NO, the exogenous NO has been effective on preventing degranulation of MCs (*i.e.*, stabilization) (20–24). Vascular intimal hyperplasia (VIH) was triggered by a shortage of NO, which is often marked by low expression of eNOS (25). Therefore, the development of a novel formulation that is capable of sustaining the NO release seems to be a viable option to maximize the atheroprotective efficacy of MCs and maintain viability of coronary artery endothelial cells (hPCAECs).

This study was aimed to explore the nanofiber-hydrogel blend (sodium alginate) containing varying combinations of S-Nitroglutathione (GSNO) (a NO donor) and Edaravone (a ROS scavenger) as a novel strategy for stabilization of MCs. Various properties of nanofiber-hydrogel composite, such as morphological and mechanical assessments, degradation and swelling rates, and the release profiles from nanofibers, were characterized to optimize the loading conditions of GSNO and Edaravone. To evaluate the effects of NO and ROS scavengers on stability of mast cells (MCs), the degranulation rates were determined by measuring the extracellular hydrogen peroxide (H_2O_2) levels and the released amount of β-hexosaminidase in the activated-MCs (a-MCs). In addition, the effects of Edaravone on the selective scavenging capacity of the oxygen radicals and prevention of peroxynitrite formation were evaluated. The effects of a-MCs (*i.e.*, pretreated with hydrogen peroxide) on re-endothelialization and viability of hPCAECs were elucidated using alamar blue and LDH assay, respectively.

MATERIALS AND METHODS

Materials

Poly (dl-lactic-co-glycolic acid) (75:25) (PLGA) was purchased from Lakeshore Biomaterials (Birmingham, AL). Sodium alginate (SA), 4-Benzoyl-3-methyl-1-phenyl-2-pyrazolin-5-one (Edaravone, EDV), Compound 48/80, Ampliflu Red, Peroxidase from horseradish type II (HRP), 4-nitrophenyl N-Acetyl-β-D-glucosaminide (p-NAG), 1,1,1,3,3,3 Hexafluoro-2-propanol (HFIP), Glutathione (GSH), and 2−7 dichlorofluorescein diacetate (DCFH-DA) were purchased from Sigma-Aldrich.

Human primary coronary artery endothelial cells (hPCAECs) (PCS-100-200), rat peripheral blood derived mast cells (RBL-2H3 or MCs), vascular cell basal medium (PCS-100-030), eagle's minimum essential medium (EMEM) (30–2003) and endothelial growth kit–VEGF (PCS-100-041) were purchased from ATCC. All other reagents and solvents were of analytical grade.

Synthesis of S-Nitroglutathione

S-Nitroglutathione was freshly synthesized using previously reported methods (26). Briefly, equimolar concentrations of sodium nitrite and GSH were dissolved in 0.5 M cold HCl. The solution was continuously stirred for 30 min at 4°C in the dark-room for protection from UV light exposure. The solution was mixed with ice-cold acetone (20 ml) and remained

under constant stirring for 30 min until it formed an insoluble precipitate (pink color) that was vacuum-filtered through 0.22 μm filter. The precipitates were washed extensively with cold pure acetone twice and cold diethyl ether once. After the washing process, precipitates were vacuum-dried and stored at −20°C until further use. The concentration of GSNO was spectrophotometrically determined at the absorbance of 340 nm.

Synthesis of Nanofiber-Hydrogel

Nanofiber-Hydrogels (NF-Gel) and Bare-Nanofibers (BNF) were produced through electrospinning techniques. The electrospinning apparatus for cardiovascular stent coating consists of a gamma high voltage supplier (Ormond Beach, FL) for an electric field (15 kV), a single syringe pump (Fischer Scientific, KS) for a constant feed rate (1.0 ml/h), a rotating motor (Grainger, MO) for stent surface coating at 1,000 rpm and 5 ml of syringe for electrospinning. The electrospinning distance between a syringe tip and collector mandrel was kept at 10 cm.

Preparation of Electrospinning Solutions

The electrospinning solution was prepared by blending a mixture of 26% (w/v) of PLGA in HFIP, 2% (w/v) of Edaravone (EDV) in HFIP, 2% (w/v) of GSNO in water and 1% (w/v) of sodium alginate (SA) in water. Briefly, the solution containing SA gel was prepared by dissolving sodium alginate (SA) (1% (w/v)) in DI water. The continuous stirring under mild heat was applied to dissolve the solutes. Once the SA was fully dissolved, GSNO (2% (w/v)) were added under continuous stirring at 4°C into the solution whose pH value was adjusted to 8.5 using 0.25 M NaOH to protect GSNO from being degraded under an acidic environment. The solution containing SA and GSNO was blended in a dropwise manner into HFIP that already had 26% (w/v) of PLGA and 2% (w/v) of Edaravone. The electrospinning solution for nanofiber-gels (NF-Gel) was stirred for 15 min until a homogeneous steady state was reached. The final concentrations of polymeric solution were 13% (w/v) of PLGA, 1% (w/v) of EDV, 1% (w/v) GSNO and 0.5% (w/v) of SA in a mixture (1 ml) of water: HFIP (1:1 ratio).

For the BNF group, GSNO was dissolved in DI water in the absence of SA. The DI water containing GSNO was blended with the polymeric solution in a dropwise manner and the rest procedures were same as described above.

Stent Coating by Electrospinning

An advanced approach to coat both inner and outer surface of stent was previously reported (27). The process was divided into two steps as shown in Fig. 1. First, electrospinning solution (1 ml) was transferred into 5 ml of syringe and then nanofibers produced by eletrospinning were deposited onto metallic wire (16 gauge and 10 cm) covered with nylon yarn. A half of solution was utilized for nanofibers fabricated on metallic wire, and cardiovascular stent was carefully inserted in the middle of deposited-nanofibers. The other half was electrospunned under the same processing conditions as aforementioned parameters. The formulations deposited onto metallic mandrel were transferred into the vacuum dryer and kept for 3 days to evaporate residual organic solvent from the nanofiber formulations. After 7 days, nylon yarn was carefully removed from the metallic wire, which made an enough space for the stents to be detached from the wire. All the samples were prepared in triplicate.

The Hardening Process of Nanofiber-Gel

NF-Gel was hardened through the crosslinking process, and the products were assigned as NF-Gel-X. The stents coated by NF-Gel were immersed in a micro-tube containing DI water (1 ml) to which 2.5% (w/v) of $CaCl_2$ was dissolved. The stents were kept in the solution for 12 h at room temperature. After the agitating process, the stents coated with NF-Gel were removed from the solution and then gently dried by the air-blow gun. It was kept in a vacuum-drying unit until the residual solution was fully evaporated from them. The dried formulations were immersed into PBS for 2 h to remove the excess amount of calcium crystals, which were built up on the surface of the formulations.

Characterization of Physicochemical Property of the Formulations

Morphological Analysis

Morphological properties were assessed by scanning electron microscopy (ESEM, XL 30, Hillsboro, OR). Specimens were sputter coated with Au-Pd, and attached to aluminum stabs with double-sided sticky carbon tape. The morphological status was examined with Field-Emission SEM (FEG ESEM XL30) at 5 kV accelerating voltage.

Mechanical Characteristics of Various Formulations

The mechanical properties of three different formulations (*i.e.* BNF, NF-Gel, and NF-Gel-X) were examined using the SSTM-5000 stress–strain analyzer (United Calibration Corporation, CA) with a 150-lb load cell. The samples were tightly attached to the grip of the analyzer using cyanoacrylate adhesive (Zapit, Dental Ventures of America, Corona, CA). A testing rate of 0.5 mm/min was applied for stress–strain measurement at room temperature (28).

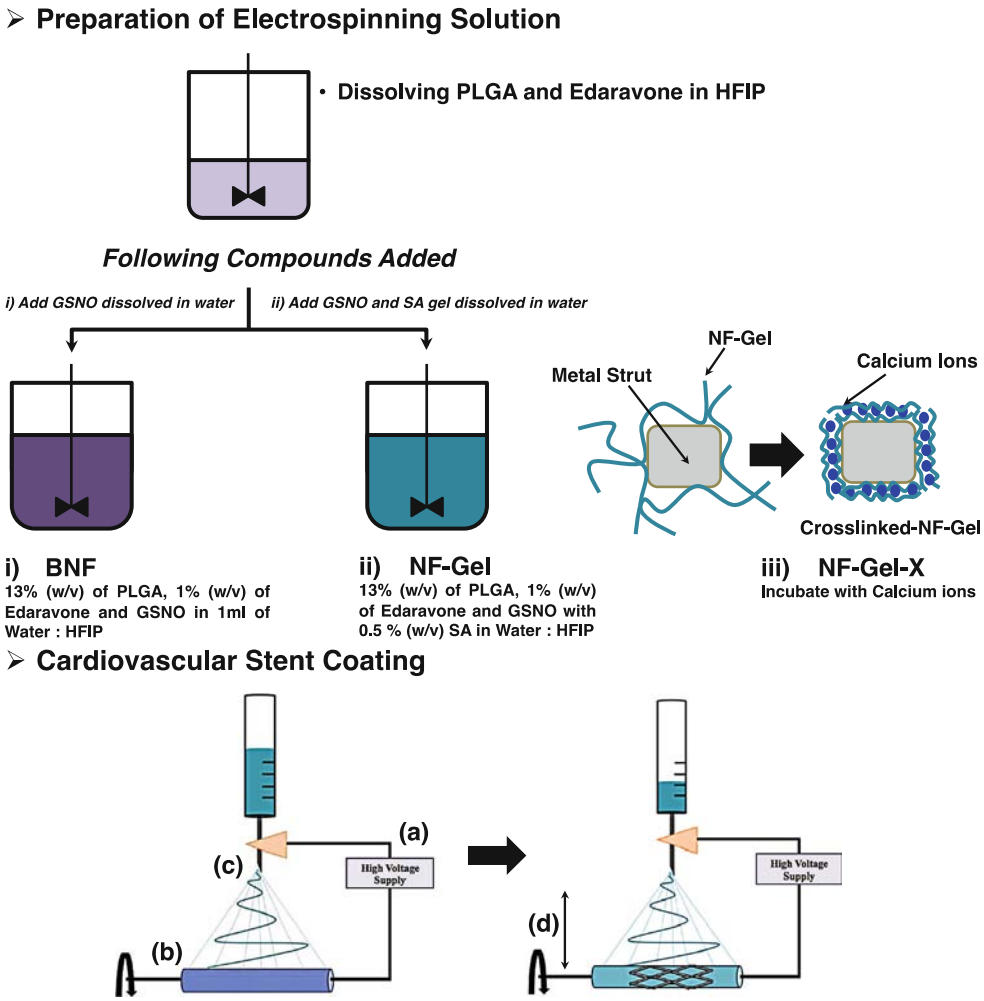

Step 1. A half of electrospinning solution was electrospunned onto the metallic mandrel covered by nylon yarn.

Step 2. Cardiovascular stent was inserted at the center of mandrel.

Step 3. The rest half of electrospinning solution was sprayed onto the surface.

Fig. 1 (*Top*) Schematic presentation of electrospinning solution, crosslinking of nanofibers-sodium alginate composite and cardiovascular stent coating. (*Bottom*) Cardiovascular stent coating under varying processing parameters (**a**) high-voltage supply (15 kV), (**b**) rotating motor (1,000 rpm), (**c**) flow rate (1.0 ml/h) and (**d**) distance between syringe tip and rotating mandrel (10 cm).

Swelling and Degradation Rates of Various Formulations

The physicochemical properties of three different formulations, such as BNF, NF-Gel and NF-Gel-X, were characterized using the methods previously utilized in our laboratory (29,30). The swelling and degradation rates of formulations were examined by comparing the water uptake capacity and biodegradability of formulations. The formulations were immersed in 1 ml of PBS with pseudo-physiological conditions as aforementioned above and the swelling rate of nanofibers was assessed. The moisture onto the formulations was gently removed using kimwipes and carefully dried by the air-blowing gun. After the weights of the swelled nanofibers were measured, the formulations were kept in a vacuum dryer for a week and dried weights were measured. The swelling and degradation rates were calculated using the following equations.

$$Swelling\ \ Rate\ \ (\%) = [(W_w - W_d)/W_d] \times 100$$
$$Degradation\ \ Rate\ \ (\%) = [(W_i - W_d)/W_i] \times 100$$

where W_i is the initial weight of polymers coated on the stent, W_w is the weight of polymers with the absorption of water, W_d is the weight of polymers free of residual moisture.

Evaluation of *In Vitro* Release Amount of Drugs

The drug release profile was spectro-photometrically monitored under the pseudo-physical conditions. Briefly, the formulations were immersed into the micro-tubes with 1 ml of PBS solution (pH = 7.4) and then kept in

the incubator equipped with a continuous rotating plate (120 rpm) at 37°C. The release media were replenished with fresh PBS solution at pre-determined time intervals. The medium was spectro-phtometrically investigated using Spetronic 20D (ThermoScientific, Waltham, MA) (Edaravone at 240 nm and GSNO at 336 nm). To determine the total amount of the drug initially loaded in each stent, the drug amount left in the stent at the end of the release study period was measured by extracting drug from the stent through the solvent-evaporation method. Briefly, the stent was immersed in PBS (1 ml) containing 200 µl of acetone. The mixture solution was probe-sonicated and kept in a vacuum chamber to completely evaporate the organic solvent. All the collected samples were gently filtered using the syringe filters (0.22 µm) and analyzed for Edaravone at a wavelength of 240 nm and for GSNO at 336 nm.

For the NO release profiles, NO produced by a thermally-induced degradation of GSNO was quantified using the Griess assay (29). Briefly, the formulations (NF-Gel-X) were incubated in PBS (200 µl) under the same conditions as described above. For the treatment group, 600 µM H_2O_2 (1 µl) was applied to PBS (200 µl) twice a day (*i.e.*, about 3 µM each). The samples were taken at pre-determined time intervals for the first 4 days and then once per week for 35 days until it reached the saturation state. The supernatant (50 µl) was placed into 96-well Plate. 1% sulfanilamide solution (50 µl) was added to each well and the plate was incubated for 5 min at room temperature. Then, 0.1% NED solution (50 µl) was added to each well. The absorbance was measured at 550 nm using the multimode detector (DTX 880, Beckman Coulter) and extrapolated to the concentration of NO (µM).

The Selective Scavenging Efficacy of Edaravone

The removal rate of ROS was assessed using the Fenton reaction to determine the scavenging efficacy of EDV (31). Various concentrations of EDV (0, 0.8, 1.2, 1.6, 2.0, 2.4 and 2.8 mM) were applied to the specific well in the presence or absence of externally added H_2O_2 (400 µM) and $FeSO_4$ (50 µM). As the equivalent volumes of both solutions were mixed in 96-well plate, the concentrations of the solutions decreased by a half (50 µM of GSNO; 0, 0.4, 0.6, 0.8, 1.0, 1.2 and 1.4 µM of EDV). The plate was incubated for 4 h at 37°C to allow H_2O_2 to be fully dissociated into hydroxyl radicals. The Griess reagent was a homogeneous mixture of two solutions; 0.1% of N-(1-Naphthyl) ethylenediamine dihydrochloride (NED) dissolved in DI water and 1% of sulfanilamide dissolved in 5% (v/v) phosphoric acid solution.

In Vitro Cell Study

Preparation of Cell Culture

To prepare the culture medium, the basal medium was properly mixed with endothelial cell growth kit-VEGF. The supplement growth kit containing rhVEGF (0.5 ng/ml), rhEGF (5 ng/mL), rhFGF basic (5 ng/ml), rhIGF-1 (15 ng/ml), L-glutamine (10 mM), heparin sulfate (0.75 Units/mL), hydrocortisone hemisuccinate (1 µg/mL), fetal bovine serum (2%) and ascorbic acid (50 µg/mL), was thawed in the water bath at 37°C. The medium was gently mixed with growth supplements and kept in the refrigerator at 4°C. hPCAECs were cultured in the medium under the standard cell culture conditions (5% CO2 and humidified air at 37°C). For the medium for MCs, EMEM was gently mixed with 15% (v/v) of heat inactivated fetal bovine serum (FBS) (Biowest LLC, MO).

Assessment of Nitric Oxide (NO) Amount

Nitric Oxide (NO) produced through cellular interaction with NF-Gel-X under oxidative stresses was quantified using the Griess assay (29). hPCAECs (10,000 cells/well) in 100 µl of the basal medium were seeded onto electrospunned nanofibers placed on the circular cover slip in a 96-well plate. The plate was incubated for overnight to allow cells to firmly attach to fiber matrix. A whole medium in the plate was transferred to the fresh 96-well plate and each well was replenished with the same volume (100 µl) of the media with or without 100 µM H_2O_2. The plate containing the medium at each well was left at room temperature to allow it to reach an equilibrium state. One percent sulfanilamide solution (50 µl) was added to each well and the plate was incubated for 5 min at room temperature. Then, 0.1% NED solution (50 µl) was added to each well. The absorbance was measured at 550 nm using the multimode detector and extrapolated to the concentration of NO (µM) that was recorded as the day-1 release amount. The NO concentrations under continuous oxidative stress were quantified every day. For the negative control, endogenous NO from hPCAECs in the absence of any drugs or oxidative stress was utilized.

Effects of Various Substrates on the Proliferation Rate of hPCAECs

Alamar Blue Assay was used to assess the proliferation rate of hPCAECs cultured on such substrates as tissue culture-treated plate (TCP) upon exposure to various formulations containing either GSNO alone or a mixture both drugs (Edaravone and GSNO) under the oxidative stress (Life Technology, CA) (32).

Briefly, cells (5,000 cells/well in 100 µl) were seeded onto TCP that was incubated (generally for 24 h) until the cells were fully fixed on the substrates. Then, the media were removed and replenished with 9% of the Alamar Blue

solution (200 μl). The plate was further incubated for 4 h to allow viable cells react with the Alamar Blue agent. The media (10 μl) from the plate were transferred to fresh 96-well plate, and then the same volume of the fresh media was added to the test plate. For the group exposed with exogenous-oxidative stress, the assigned wells were refilled with 100 μM of H_2O_2 (10 μl). 10 μl each of the test medium was transferred to fresh 96-well plate already filled with the fresh media (90 μl). The fluorescent intensity of 100 μl of the solution was measured using the multi-reader plate (Ex: 540 nm and Em: 590 nm). The proliferation rates were determined every other day and the fluorescent intensities were normalized with respect to those at day 1.

Analysis of Reactive Oxygen Species (ROS) Produced by Activated-Mast Cells

Intra- and extracellular ROS induced by the sensitizer, the compound 48/80 (c48/80), was analyzed using a ROS-sensitive fluorescent dye. For the extracellular ROS generation, Amplex™ Red with horseradish peroxidase (HRP) was utilized. Briefly, MCs (2.0×10^4 cells/well) in EMEM (100 μl) were seeded onto the black 96-well plate, which was incubated for overnight to allow cells to attach to the bottom of the plate. After incubation, each well was gently washed with DPBS twice. Four different concentrations (0 ng/ml as the control, 100 ng/ml, 200 ng/ml and 300 ng/ml) of c48/80 in vascular basal media (50 μl each) were added to each well already filled with 50 μl of working solution (4.93 ml of DPBS, 20 μl of 20U HRP and 50 μl of 10 mM Amplex™ Red). Thus, the final concentration of c48/80 was reduced down to a half when both solutions were mixed.

For generation of intracellular ROS, the inter-cellular ROS level was determined using a ROS specific fluorescent dye (DCFH-DA). MCs (2.0×10^4 cells/well) in 100 μl of EMEM was seeded onto the black 96-well plate and incubated for overnight. The residual media were removed and 25 mM DCFH-DA solution (100 μl) equivalent to the subcellular level concentration was added to each well. The plate was incubated for 35 min to allow the dye to pass through the cellular membrane. Then, the dye solutions were removed and the plates were mildly washed once using DPBS. Four different concentrations of c48/80 (0 ng/ml as the control, 50, 100 and 150 ng/ml) were added to the plate.

Both plates were read using the multi-reader plate at predetermined time intervals: 5 min, 15 min, 30 min, 1 h, 6 h, 10 h, 15 h and 24 h (for Amplex™ Red, Ex: 530 nm and Em: 590 nm; For DCFH-DA, Ex: 485 nm and Em: 535 nm). The relative ROS levels were calculated based on the fluorescent intensities and expressed as the ratio between two readings (the reading at the specific time and the reading at 0 min) (*i.e.*, Relative ROS Levels = the fluorescent reading at predetermined time intervals divided by the fluorescent reading from the first reading (0 min)). The ratio is utilized to describe the changes in the ROS levels from the initial value.

Assessment of Degranulation of Sensitized-Mast Cells (MCs)

The MCs were seeded on the 24-well plates (3.0×10^4 cells/well), that were further incubated for 24 h to allow cells to attach to the bottom of the plates. Once the cells were confluent, the medium was replaced with the basal medium containing 150 ng/ml of c48/80. The degranulation rate of activated-mast cells was assessed using the activity of β-hexosaminidase, a granule-stored enzyme secreted into the cell supernatant (9). The aliquots (10 μl) of each sample were taken from 24-well plate at predetermined time intervals (1, 10, and 24 h) and then transferred into the fresh 96-well plate already containing an equal amount of 1 mM of p-NAG. The 96-well plate was incubated at 37°C for 1 h, and 250 μl of Na_2CO_3/$NaHCO_3$ were added into each well. The absorbance was read at 400 nm using a multimode detector. To quantify the total amount of β-hexosaminidase in cells, the following procedure was performed. In brief, 2% Triton X-100 (10 μl) was added to lyse cells. After 20 min, the medium containing cell debris was centrifuged at 9,000 rpm for 2 min. The aliquots (10 μl) of lysate solution were sampled to measure the total amount of β-hexosaminidase (*i.e.*, considered as 100% degranulation). The released amount in the supernatant was calculated and expressed as the percentage value (%), as the amount of β-hexosaminidase in the supernatant was divided by the total amount of β-hexosaminidase in the lysate solution.

Evaluation of Cytotoxicity of Sensitized-MCs on hPCAECs

To evaluate cytotoxicity of activated-MCs on hPCAECs, LDH assay (CytoTox-ONE™ Homogeneous Membrane Integrity Assay, Promega Co.) was performed on the transwell co-culture system as depicted in Fig. 2. Briefly, hPCAECs (1.0×10^5 cells/well) in the basal media (1 ml) were seeded onto electrospunned nanofibers placed on circular cover slip (18 mm circles, VWR Scientific) in a 12-well plate. MCs (3.0×10^4 cells/well) in 500 μl of EMEM were seeded onto 12 mm transwell inserts (0.4 μm pore polycarbonate membrane, Corning) and transferred into 12-well plate containing 1 ml of EMEM. Both 12-well plate containing hPCAECs and transwell inserted-12-well plate containing MCs were incubated separately overnight to allow the cells to attach to the bottom of the plate. Once both cells were confluent, the medium was removed and the insertions containing MCs were combined with 12-well plate in which hPCAECs were confluent. MCs were sensitized using c48/80 (150 ng/ml in the basal media).

The plate of the co-culture system was incubated for 48 h under the standard culture condition. Each medium (100 μl)

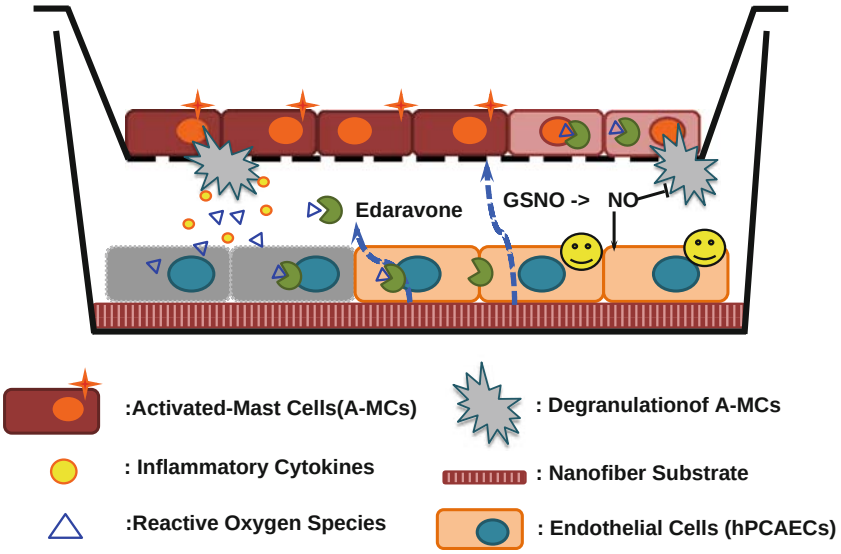

Fig. 2 Schematic presentation of the transwell-insertion.

from the insertion wells and bottom wells was transferred into the fresh 96-well plate at pre-determined time intervals (24 h and 48 h incubation), that was subsequently mixed with LDH reagent. The same amount of the medium was refilled into the wells. The fluorescent intensity (Ex: 560 nm, Em: 590 nm) of the 96-well plate was read using the multimode detector.

For the assessment of the inhibitory efficacy of degranulation by exogenous NO, the β-hexosaminidase levels in the media (10 μl) from the insertion wells were determined at pre-determined time intervals.

Statistical Analysis

Data were presented as mean ± standard deviation (SD). Independent *t*-test was used to compare the means of two independent samples. P value was determined using SPSS software (SPSS, Chicago, IL) and P values of less than 0.05 were reported as statistically significant. All experiments were conducted in triplicate and repeated at least three times.

RESULTS AND DISCUSSION

Preparation of Cardiovascular Stent-Coated by Nanofiber-Hydrogel

Nanofiber-hydrogel composites produced by electrospinning technique were evaluated for the surface coating efficacy of the cardiovascular stent (Fig. 1). As described in Table I, three different coating groups were applied onto metallic substrates. Each group has unique characteristics including different morphologies and varying amounts of incorporated drugs in the polymer matrix. The weight amount of polymer matrix coated on the external/internal sides of NF-Gel stent was greater than that of BNF (3.53±0.6 mg for BNF and 4.38±0.13 mg for NF-Gel). It was previously demonstrated that the electrospinnability increased, as the concentration of HFIP decreased in the co-solvent system. The enhancement of the matrix mass per stent may be due to higher viscosity of the co-solvent system (water: HFIP, 50:50), leading to enhanced electrospinnability and subsequently resulting in the greater amount of polymeric matrix per stent (*i.e.*, higher than the compositional ratio).

It was found that there was a significant loss of GSNO in NF-Gel-X during the hardening process, whereas there was no significant loss of EDV. NF-Gel immersed in the $CaCl_2$ solution for the crosslinking process may cause GSNO, a hydrophilic compound, to be partially degraded in nanofibers. In addition, the weight amount of cross-linked NF-Gel-X was greater than NF-Gel due to the absorption of calcium (Ca^{++}) to sodium alginate.

Morphological Assessment of Nanofiber Formulations

The morphology of nanofiber formulations was assessed using SEM analysis to determine the structural variation of nanofibers. As shown in Fig. 3b and Table I, the mean diameter distribution of three nanofiber formulations (*i.e.*, BNF, NF-Gel and NF-G-X) ranged from 200 nm to 1.1 μm that was significantly affected by the amount of sodium alginate during the blending process. The mean diameter of cross-linked alginate gel (1097.5±417.2 nm for NF-G-X) was greater than both BNF and NF-Gel (329.17±193.7 nm for NF-Gel), because the connection of alginate with Ca^{++} ions occurred at the outer layer of nanofibers that was confirmed by the magnified images (Fig. 3c). As compared to BNF and NF-Gel (left and middle in Fig. 3c), the space denoted by star markers within NF-G-X was narrow and compact. It was concluded that the blending process greatly affected the morphology of

Table I Characterization of Various Test Formulations

	Amount of loaded-drug per stent (μg)		Amount of polymeric matrix per stent (mg)	Diameter distribution (nm)
	Edaravone	GSNO		
Bare-NF[a]	137.7 ± 6.6	182.3 ± 19.8	3.53 ± 0.6	198.54 ± 66.1
NF-Gel[b]	154.3 ± 2.7	185.9 ± 8.9	4.38 ± 0.13	329.17 ± 193.7
NF-Gel-X[c]	143.6 ± 7.2	125.4 ± 12.4	4.62 ± 0.1	1097.5 ± 417.2

Data are shown with Mean ± S.D. ($n = 3$)

[a] 13% (w/v) of PLGA

[b] 13% (w/v) of PLGA + 0.5% (w/v) of sodium alginate (SA)

[c] NF-G-X represents the formulation of cross-linked NF-Gel

the nanofiber and the crosslinking process generated the bulky but a tighter and compact space within nanofibers.

Mechanical Properties of Nanofiber Formulations

For the assessment of physicochemical properties, the elongation, degradation, and swelling rates were examined using the previously utilized methods (19,33). Because cardiovascular stent needs to be expanded during the angioplasty process, the elongation rate of nanofibers was measured as a compulsory property. As shown in Fig. 4, the elongation rates of nanofibers blended with sodium alginate (NF-Gel and NF-Gel-X) were much greater than those of PLGA-nanofibers (BNF) (Fig. 4a). Once sodium alginate was bound with Ca^{++} ions, the elongation rate of NF-Gel-X was reduced, but was still greater than that of BNF.

Evaluation of Physicochemical Properties of Various Formulations

To further elucidate the changes in physicochemical properties induced by the blending process with sodium alginate, the degradation and swelling rates of those formulations were determined. As shown in Fig. 4b and c, the crosslinking process enhanced the degradation rate of all formulation types, and the degradation profile reached an equilibrium status in about 14 days. It was reported that the dissolution of the alginate nanofibers cross-linked with bivalent metal ions, such as Ca^{++}, Ba^{++} or Sr^{++}, occurred as a result of the exchange between Na+ ions and Ca^{++} ions that formed salt bridges (34,35). NF-Gel-X group showed the fast degradation rate in the first 2 weeks. However, in biological system, the ion exchange rate is maintained at a lower level than those in the PBS, so the intercalated Ca^{++} within alginate chains remained stable for the extended period of time. Subsequently, NF-Gel-X can maintain integrity of polymeric fiber for a prolonged time period. Although the removal of deposited calcium was attempted, it may be possible that there was a trace amount of calcium crystal remained in the surface of nanofibers that may have a direct impact on the degradation rate. Thus, it is integral to thoroughly remove the calcium through the proper procedure.

It was found that the swelling rate for the formulations composited with hydrogel during the incubation for 1 day was faster than that for BNF group (4.9 ± 1.2% for BNF, 18.5 ± 4.9% for NF-Gel and 14.6 ± 1.5% for NF-Gel-X). However, there were no significant differences in the swelling rates between BNF, NF-Gel and NF-Gel-X for 5 weeks. Nanofibers of NF-Gel and NF-Gel-X prepared using the blending techniques (*i.e.*, the composites of PLGA and SA) may yield the enhanced therapeutic efficacy *via* increased elongation rates in the blood vessels when they are applied to angioplasty surgery.

In Vitro Release Profiles of Loaded Drugs

The drug release studies were performed over a period of 35 days under the pseudo-physiological conditions. The cumulative released profiles of a ROS scavenger (Edaravone, EDV) and a NO donor drug (GSNO) from the formulations of BNF, NF-Gel and NF-G-X were compared in Fig. 5.

EDV from the formulations showed greater sustained release pattern over a period of 5 weeks. There was a burst release of EDV for the first day in the release profiles that gradually reached a plateau. In addition, the composition of the formulations significantly affected the cumulative released amount of EDV. For NF-Gel, the released amount up to 35 days was 21.5 ± 1.1%, that was significantly smaller than that of BNF (36.1 ± 4.3% at 35 days) ($p < 0.05$, $n = 3$). Although an initial loss of EDV from NF-G-X during the crosslinking process was still observed (Table I), its release rates were significantly slowed as compared to those of both BNF and NF-Gel (5.7 ± 0.2%, $p < 0.01$, $n = 3$). The intercalated-SA caused EDV to be stabilized and remained intact for the extended period of time, yielding its sustained release profiles from nanofiber-based matrix. The outer layer of NF-G-X composed of sodium alginate-gel prevents EDV from being directly exposed to the environmental solution, thus protecting them for a longer period of time.

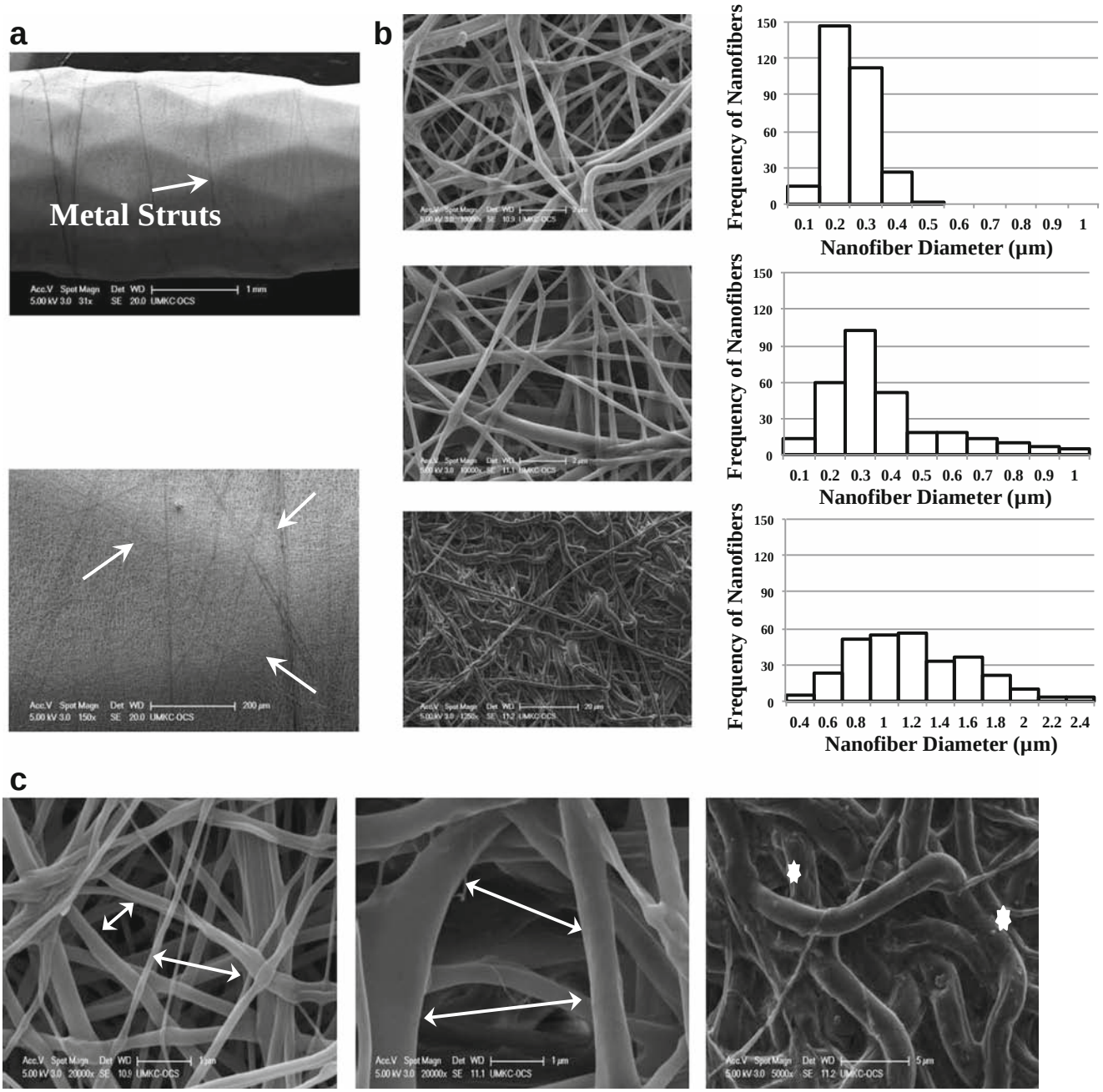

Fig. 3 Morphological characteristics of various nanofibers consisting of Poly (dl-lactic-co-glycolic acid) (75:25) (PLGA) and Sodium Alginate (SA). (**a**) SEM results of stent- surface coated with nanofiber. *Top*, the side view of stent. *Bottom*, the magnified-side view of stent. *White arrow* point to metallic struts. (**b**) SEM images of three nanofiber formulations. *Top*: Bare-Nanofibers (BNF), Poly (dl-lactic-co-glycolic acid) (75:25) (PLGA) only; *Middle*: NF-Gel, PLGA blended with SA; *Bottom*: NF-G-X. (**c**) Magnified-SEM images. *Left*: BNF; *Middle*: NF-Gel; *Right*: NF-G-X. *Double-head arrow* indicated the space between nanofibers (BNF and NF-Gel). Marks on NF-G-X point out the shrinkage of space after the crosslinking process.

The release profiles of NO donors (GSNO), a hydrophilic compound, were further assessed for the characterization of nanofibers blended with alginate hydrogel. As shown in Fig. 5b, it was found that almost 50% of GSNO were released from BNF in 3 days, whereas the sodium alginate blended formulations (NF-Gel) displayed a significantly sustained release profile of GSNO, taking a week to release 50% of the total amount of initially loaded GSNO. The release rate of GSNO from NF-G-X showed a similar pattern to those from both BNF and NF-Gel for the first day of incubation, but,

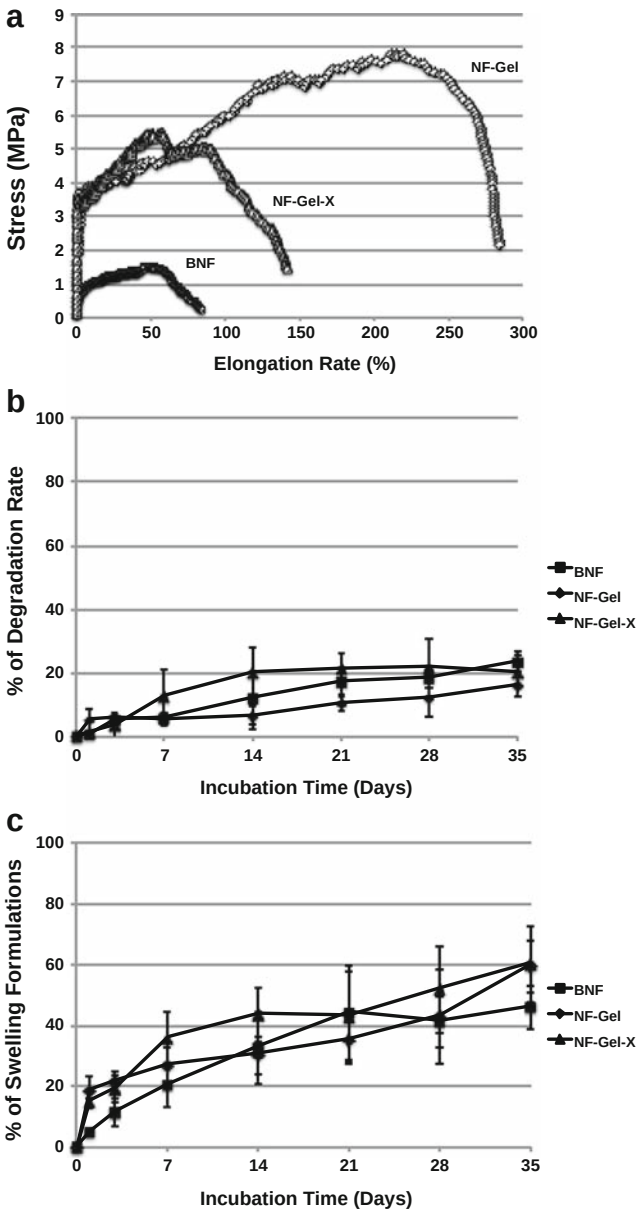

Fig. 4 Physicochemical characteristics of nanofiber formulations. Mechanical property curve (**a**), Degradation rate (**b**) ($n = 3$) and swelling rate (**c**) ($n = 3$).

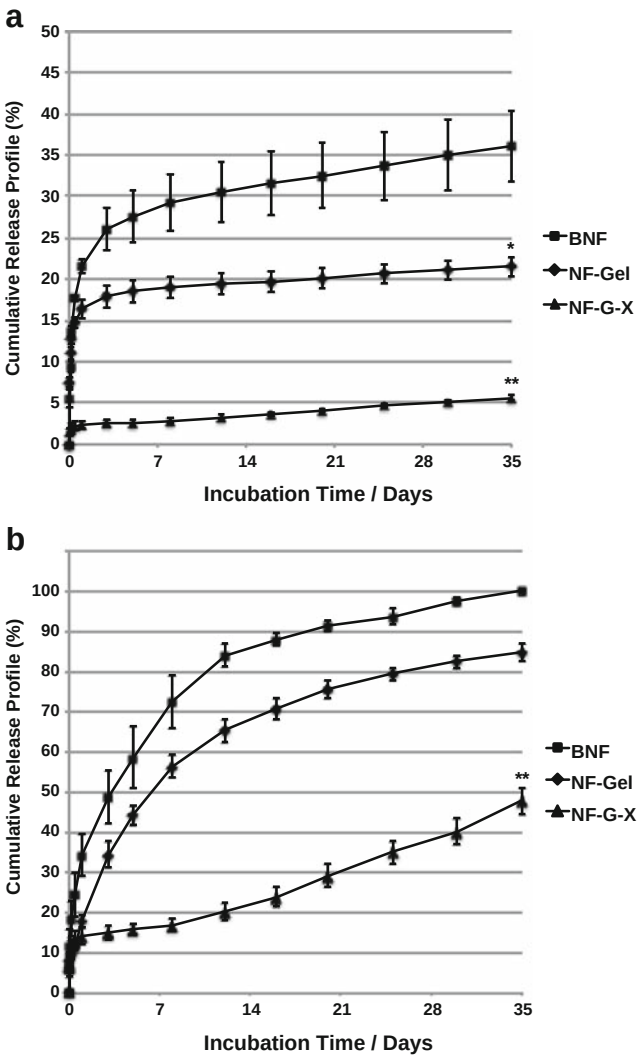

Fig. 5 The cumulative released amount of Edaravone and S-Nitroglutathione (GSNO). (**a**) The release profiles of Edaravone (**b**) the release profiles of GSNO (* and ** denotes statistically significant difference at $p < 0.05$ and $p < 0.01$ compared to the results of BNF, respectively, $n = 3$).

after that point, the release rate of GSNO from NF-G-X was much slower than those from both BNF and NF-Gel groups. These results support that the release rates of loaded drugs from nanofibers can be slowed down by being blended with hydrogel and the subsequent crosslinking process.

Effects of ROS on Production of NO

The scavenging efficacy of Edaravone (EDV) was evaluated by assessing the changes in the amount of NO in the system. The assessment of NOx (any degraded products of nitric oxide metabolites such as NO_2 or NO_3) by the Griess assay has accurately reflected the nitric oxide production (36,37). It was found that the amount of NO produced in the system decreased, as the concentration of EDV increased, indicating that the amounts of NO were significantly affected by the oxidative stress imposed on the experimental system.

As shown in Fig. 6a, EDV treatments (~1.0 mM) had a significant impact on changes in the NO concentrations under the oxidative stress. The effects of EDV on the production of NO were greatly influenced by the presence of superoxide or hydroxyl radicals in the system. It was shown that the NO level significantly decreased in the absence of oxidative stress, that is in accord with previous reports including suppression of the NOx levels in neonatal hypoxic/ischemic brain damage by EDV (36). The scavenging activity of EDV was potent and highly selective to superoxide or hydroxyl radicals (37).

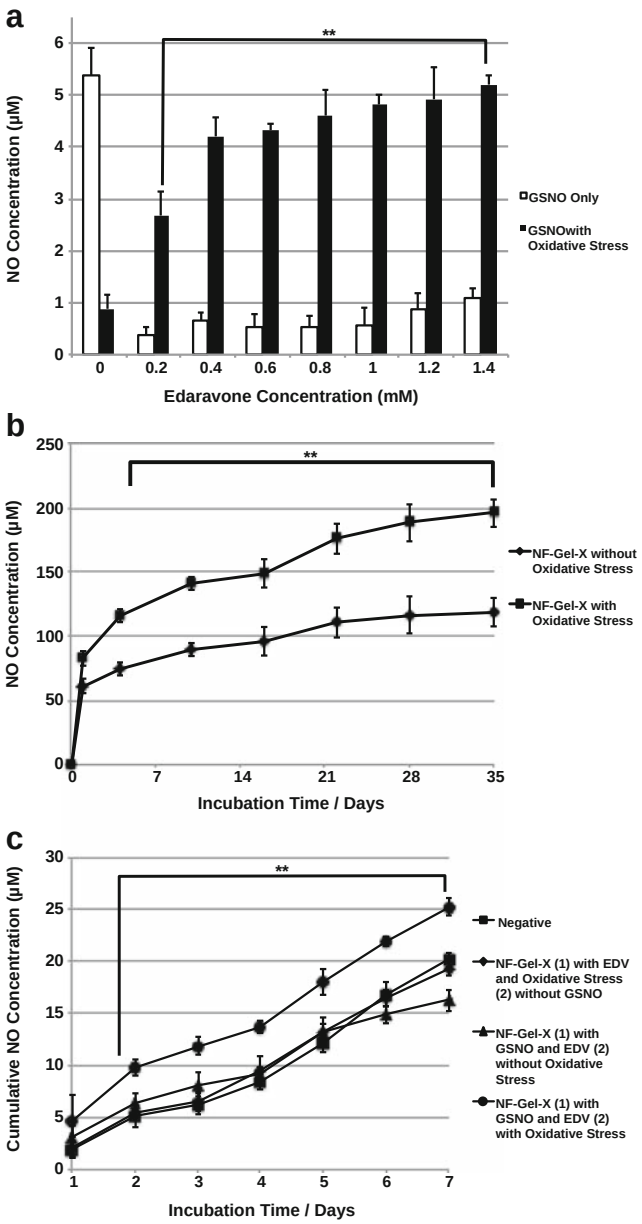

Fig. 6 Scavenging efficacy of Edaravone. (**a**) The Nitric Oxide (NO) amount induced by thermal degradation of GSNO under various conditions (**b**) The cumulative amount of NO from NF-G-X under pseudo-physiological condition with/without oxidative stress. (**c**) *In vitro* NO amount (** indicated statistically significant difference at $p < 0.01$ compared to the results of the groups without oxidative stress, $n = 3$).

As shown in Fig. 6b, it was found that the NO level under the continuous oxidative stress was higher than that without oxidative stress. The significant difference in the NO concentration levels during the entire treatment period of 35 days indicated that NO donor-eluted stent could overcome endogenous oxidative stresses produced by a-MCs or oxidized-low density lipoprotein (ox-LDL) in atherosclerosis lesion. It is highly likely that the high level of NO suppresses the formation of peroxynitrite ($ONOO^-$) (*via* consuming oxygen) that has been considered as strong radicals and has negative effects on vascular endothelial cells. Therefore, co-administration of a radical scavenger (*i.e.*, EDV) appears to be a promising strategy to reduce the ROS-mediated immune responses.

The concentration of NO produced *via* interaction between hPCAECs and NF-G-X for a week was assessed and compared with the negative control group as a baseline, because NO could be inherently produced by hPCAECs. As shown in Fig. 6c, NF-G-X containing EDV and GSNO under conditions of oxidative stress induced by exogenous compounds produced the higher level of NO than the negative control group, indicating that EDV could capture oxygen radicals and maintained higher viability. Furthermore, it was demonstrated that the production of NO from NF-G-X containing only EDV (without GSNO) under oxidative stress conditions was similar to that from the negative control. The concentrations of NO from NF-G-X containing both drugs (EDV and GSNO) under no oxidative stress conditions showed a similar pattern to that under oxidative stress conditions. ROS could trigger the production of peroxynitrite in the presence of NO that stimulated the apoptosis of vascular endothelial cells. However, when the radical scavenger (EDV) was co-administered, the level of ROS decreased, because EDV could scavenge both oxygen and peroxynitrite radicals.

Proliferation of hPCAECs on Various Substrates

The effects of various substrates on the proliferation rate of hPCAECs were evaluated using Alamar Blue assay. The fluorescent unit measured on the first day was utilized to normalize the fluorescent data analysis. As shown in Fig. 7, the amount of NO released from NF-G-X containing GSNO significantly enhanced the proliferation rate of hPCAECs as compared to those from NF-G-X without GSNO ($p < 0.01$ at 3, 5, and 7 day). Because the formulations had no scavenger (*i.e.*, EDV) in them, an increase in NO concentration could trigger rapid re-endothelialization on hPCAECs.

The study on the effects of drugs ([a]: EDV and GSNO combination) on the proliferation rate of hPCAECs analyzed by fluorescent units (RFUs) demonstrated that the oxidative stress has a major impact on the proliferation rate ($p < 0.01$ at 3 and 5 day, $p < 0.05$ at 7 day), indicating that NO derived by GSNO could act as a catalyst to enhance re-endothelialization. Because the concentration of NO was lowered by the radical scavenger in the absence of oxidative stress, the display pattern of the RFUs was similar to that of NF-G-X without GSNO. On the other hand, the proliferation rate of NF-G-X containing a mixture of GSNO and EDV under oxidative stress yielded rapid endothelialization. Thus, nanofibers incorporated with a mixture of EDV and GSNO seem to be a suitable platform for coating the surface of endovascular stent, accomplishing rapid endothelialization of cells migration onto stent surface.

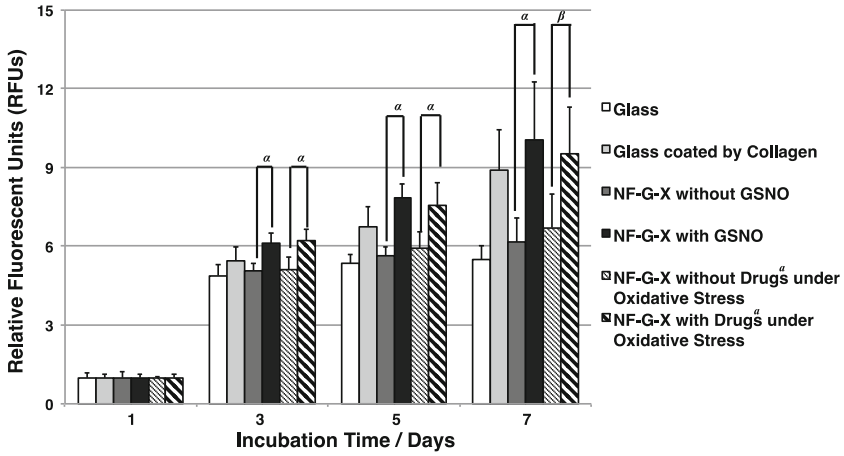

Fig. 7 Effects of a mixture of GSNO and Edaravone on the re-endothelialization rates of hPCAECs. (α and β indicates significant differences between two groups at $p < 0.05$ and $p < 0.01$, respectively, $n = 3$).

Assessment of ROS Production by Activated Mast Cells (a-MCs)

The amounts of intracellular and extracellular ROS produced by activated mast cells (a-MCs) were evaluated using the previously reported method (38,39). Mast cells (MCs) were activated using varying concentrations (0, 50, 100 and 150 ng/ml) of the compound 48/80 (c48/80).

For the assessment of intracellular responses to oxidative stress, fluorescent intensity of oxidized-DCF was measured using the multi-reader plate at predetermined time intervals. As shown in Fig. 8a, the level of oxidized-DCF was significantly greater than that of the control. It was also demonstrated that the ROS levels analyzed based on fluorescent intensity at the subcellular level during 1 h incubation of all treatments were greater than the initial reading by about 2 folds. As the concentration of c48/80 increased, the fluorescent intensity also increased after 1 h and reached a plateau after 10 h treatment. In all treatment groups, the levels after 10 h treatment were greater than the initial reading by about 3 folds, whereas it was greater than the initial reading by about 2.5 folds in the control group.

The amount of hydrogen peroxide (H_2O_2; ROS) generated by a-MCs upon exposure to c48/80 (150 ng/ml) was measured using Amplex™ Red reagent (Fig. 8b). There were no significant changes in the amount of H_2O_2 until incubation for 3 h, however, since then the fluorescent intensities reflecting the amount of H_2O_2 of the treatments groups continuously increased, as the c48/80 concentration increased. The amounts of H_2O_2 of the treatment groups were significantly greater than the control group after 6 h incubation. The amounts of H_2O_2 from the treatment groups with 100 and 150 ng/ml for 27 h were greater than those from the control by about 4 and 5 folds, respectively.

In addition, the fluorescent images taken by fluorescent microscopy (Leica DMI 3000D, IL) displayed the enhanced bright field inside cells as shown in Fig. 9. Since the treatment with 150 ng/ml showed the highest enhancement of oxidative stress, the concentration of 150 ng/ml was chosen for further studies. The intensity of the bright fields marked by white

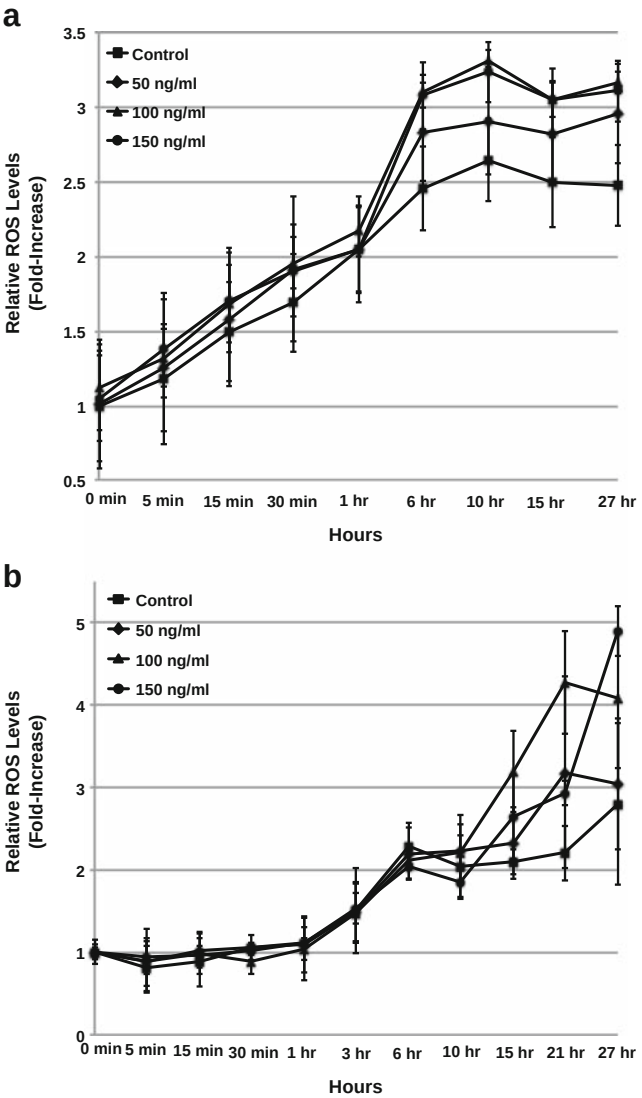

Fig. 8 The levels of ROS stimulated by the compound 48/80 (c48/80). (**a**) The subcellular ROS level. (**b**) The exogenous level of ROS ($n = 6$).

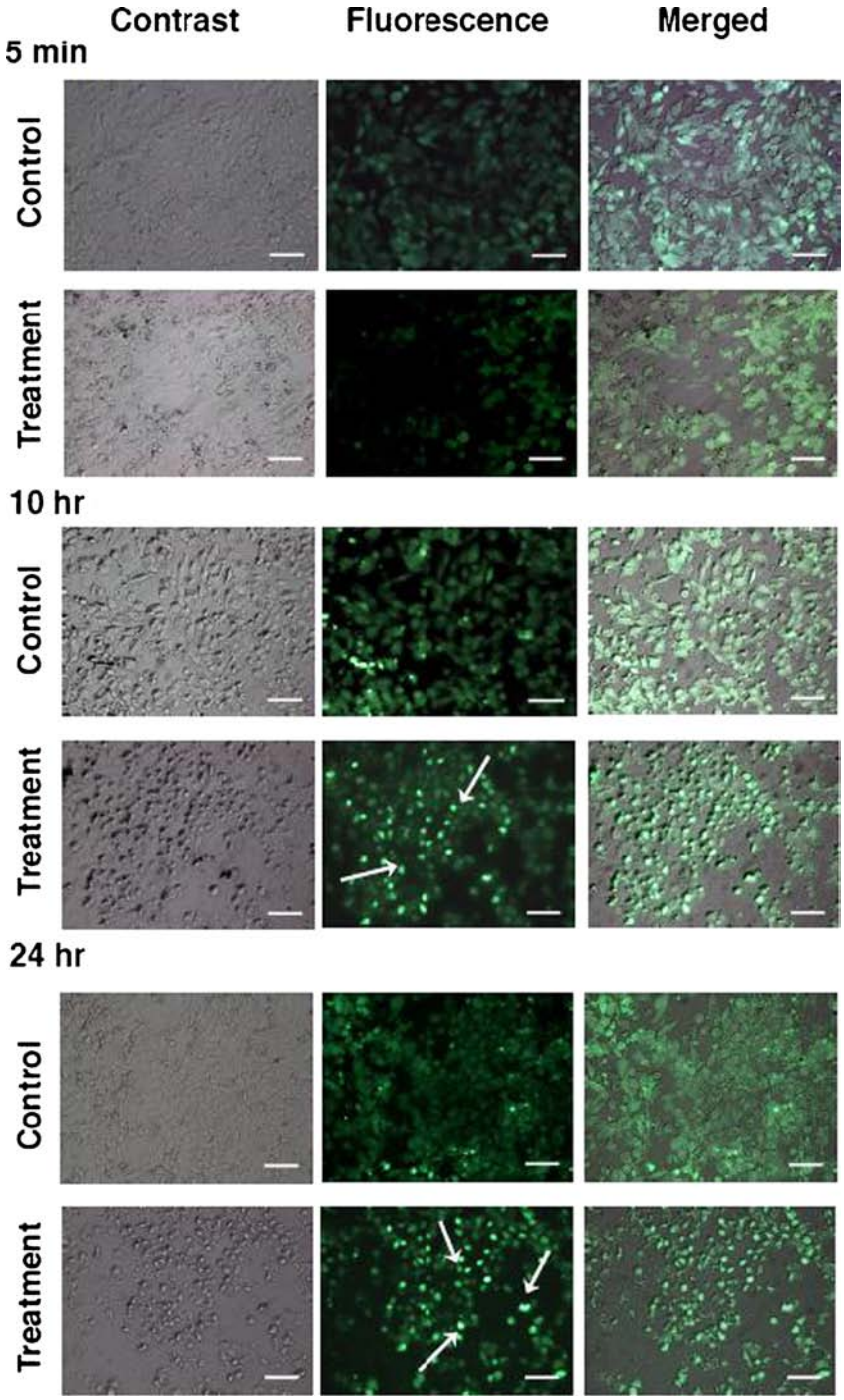

Fig. 9 The endogenous ROS level activated by c48/80 (150 ng/ml) and traced by DCF-DA dye. *White arrows* point to bright fields exerted by the interaction between DCF-DA and ROS. All scale bars indicate 100 μm.

arrows in the treatment group for 10 h incubation is similar to that for 24 h. For the control groups, it was difficult to detect the bright field throughout the incubation period.

The oxygen radicals released from the degranulated mast cells were converted to H_2O_2 by SOD present in the degranulated mast cells (15). It was observed that the level of H_2O_2 in the extracellular medium increased, as the intracellular level of H_2O_2 increased. After incubation for 15 h, the degranulation of a-MCs was observed and various byproducts, such as inflammatory cytokines and histamine, were released from them. Therefore, the stabilization of a-MCs seems to be a key factor to the successful application of angioplasty.

Effects of the Compound48/80 on Degranulation of MCs

Degranulation of a-MCs was monitored with the release profiles of two different mediators, granule-associated β-hexosaminidase and histamine. A significant discrepancy

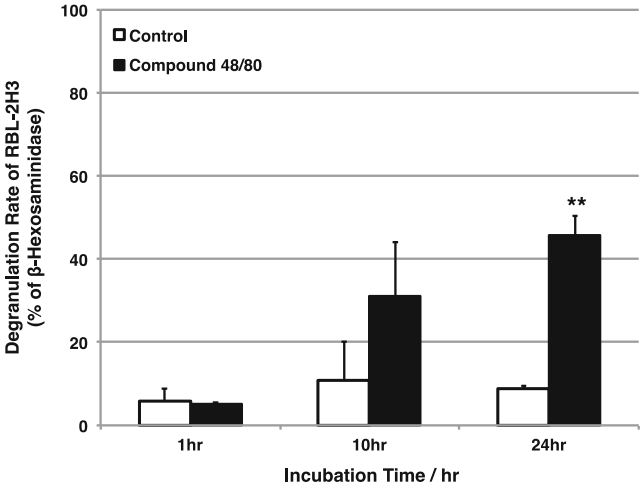

Fig. 10 The β-Hexosaminidase level assessed for exocytosis of mast cells induced by compound 48/80 (** denotes statistically significant difference at $p < 0.01$ compared to the control group, $n = 3$).

in degradation outcome was previously reported mainly due to the fact that the fluorometric assay has not been selective for histamine alone, but reacted with other amines to give fluorescent adducts (40). MCs appeared to be a reliable model to study IgE-mediated degranulation of secretory cells, exhibiting a bell-shaped dose–response curve as a function of anti-DNP IgE concentration (41).

To evaluate the exocytic response of MCs stimulated by c48/80, the amount of β-hexosaminidase released into the supernatant was quantified at pre-determined time intervals (1, 10, and 24 h) (9). As shown in Fig. 10, the level of β-hexosaminidase gradually increased as a function of time. However, for the control group, no changes in the degranulation rate were observed during the same period. The degranulation rate at 24 h (45.8±4.5%) in the testing group was significantly greater than that in the control group (8.9±0.7%, $p < 0.05$ ($n = 3$)).

Effects of Exogenous Nitric Oxide (NO) and ROS Scavengers on Sensitized MCs

The efficacy of a mixture of NO donors and ROS scavengers on degranulation of a-MCs and viability of hPCAECs were investigated using alamar blue and LDH assay, respectively. As shown in Fig. 11a, there were no significant cytotoxic effects of GSNO and Edaravone on the viability of hPCAECs. The compound 48/80 (c48/80), a sensitizer to induce ROS, at all tested concentrations didn't affect the viability of a-MCs (Fig. 11b). The results of this study were closely correlated with previous findings, in which the degranulation of mast cells were accelerated without affecting the viability of MCs, when MCs were activated by Ag+ (42).

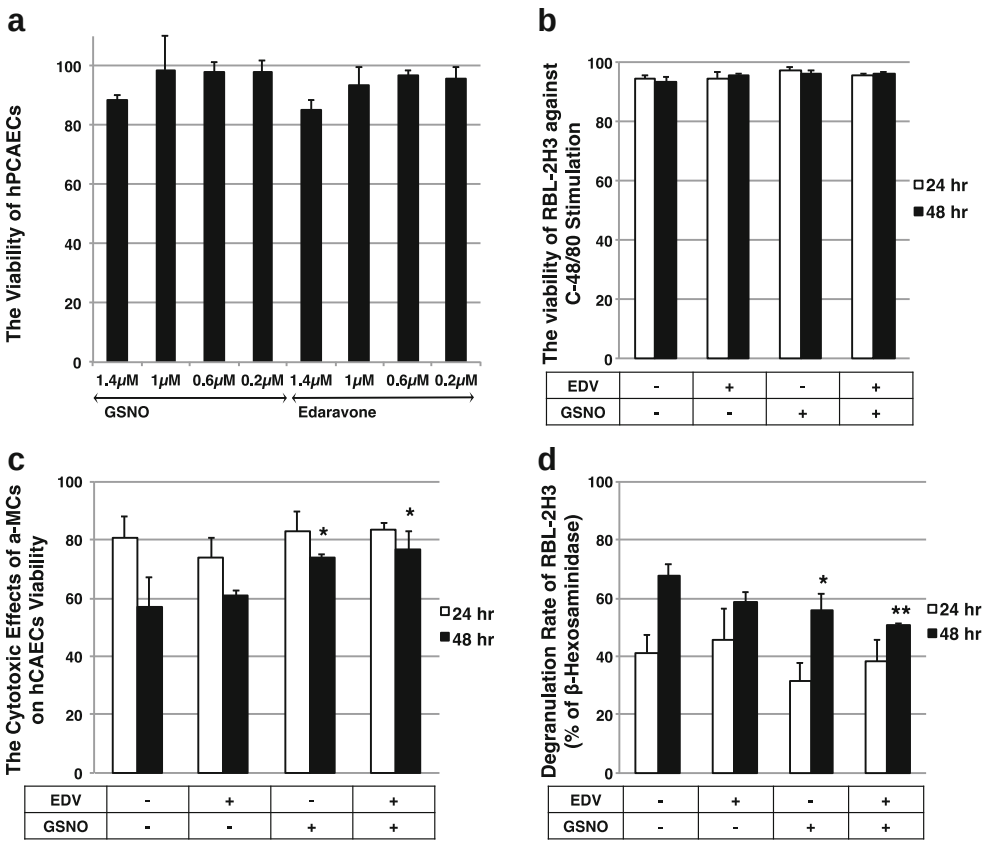

Fig. 11 Effects of a mixture of GSNO and Edaravone on the viability of hPCAECs (**a**) The viability of hPCAECs at different concentrations of GSNO and Edaravone (**b**) the viability of a-MCs against the exocytic substances for 24 h and 48 h (**c**) the cytotoxic effects of ROS on the viability of hPCAECs. (**d**) The β-Hexosaminidase level of activated-mast cells in the presence or absence of Edaravone and GSNO for 24 h and 48 h incubation. (* and ** indicated a significant difference at $p < 0.05$ and $p < 0.01$ compared to the negative control group at 48 h, respectively, $n = 3$).

It was reported that the exocytic substances containing cytokine secretion and hydrogen peroxide by a-MCs played an essential role in the viability of hPCAECs (43). As shown in Fig. 11c, the control group (hPCAECs without any drug treatments) showed the lowest viability of hPCAECs owing to the degranulation of a-MCs (80.5±7.2% for 24 h incubation and 56.7±10.1% for 48 h incubation by a-MCs). EDV applied to the system had no significant effects on the viability of hPCAECs (73.6±6.7% for 24 h and 60.9±1.9% for 48 h incubation). However, both GSNO group and the group containing a combination of GSNO and EDV significantly enhanced the viability of hPCAECs after incubation for 48 h (73.7±1.3% and 76.5±5.4%, respectively) mainly due to the stabilization of a-MCs by exogenously delivered NO from the exocytic substances. As shown in Figs. 6 and 11c, the efficacy of EDV on MCs stabilization decreased, as the level of NO in the system decreased, subsequently enhancing the cytotoxic response of hPCAECs.

To evaluate the inhibitory efficacy of exogenously delivered NO on the degranulation of MCs, the β-hexosaminidase levels were measured from MCs loaded in transwell as designed in Fig. 2. Although it is still in dispute whether or not mast cells produce NO, it was previously demonstrated that mast cell degranulation was inhibited by exogenous NO (20,44). The exocytic expression of a-MCs increased as incubation time increases (% of β-hexosaminidase, 41.3±6.2% for 24 h and 67.8±3.7% for 48 h incubation). The degranulation rate reflected by the amount of β-hexosaminidase decreased, as a-MCs were treated with either GSNO or a mixture of GSNO and EDV. For the EDV treatment group, the amount of β-hexosaminidase remained constant.

GSNO alone or a mixture of GSNO and EDV significantly lowered the degranulation rate of a-MCs (GSNO only: 55.8±5.4%; GSNO with EDV: 50.6±0.6%), indicating that NO plays a major role in degranulation of a-MCs (Fig. 11c and d). The efficacy of a combinatory approach of GSNO and EDV on the ROS-mediated immune responses from activated-MCs was validated by demonstrating the balance between NO and ROS, stabilizing the atherosclerosis lesion, and enhancing the viability of hPCAECs.

It is noteworthy that as in the early days of the fiber-based stent, however, enthusiasm for these techniques needs to be supplemented by apprehension of potential risks, the extent of which has not been identified. Moreover, it should be investigated that endothelial progenitor cells or bone-marrow derived stem cells are effectively migrated onto the nanofiber substrates against blood flow. Therefore, the development of culture systems that allow stem cells to proliferate and survive as stem cells with no potential side effects should be a prerequisite for extensively application of the fiber-based stent to the treatment of CAD.

CONCLUSION

Nanofiber having an utmost porous structure could provide a large surface area for diffusion, rendering stents a desirable release profile. Advanced cardiovascular stent coated with nanofiber containing a mixture of nitric oxide donors and ROS scavengers could be used as a promising strategy to protect mast cells (MCs) from the ROS-mediated immune response. This approach will ensure the viability of vascular lining against the degranulation of activated-MCs, thus providing a novel method to protect the atherosclerosis lesion and progress of CAD. The enormous feasibility of this approach has been demonstrated, and it can be anticipated that these techniques will be adapted in numerous clinical trials in the near future.

ACKNOWLEDGMENTS AND DISCLOSURES

This study was supported by Missouri Life Science Research Board Grant (09–117).

REFERENCES

1. Kabir AM, Selvarajah A, Seifalian AM. How safe and how good are drug-eluting stents? Future Cardiol. 2011;7:251–70.
2. Teirstein PS. Drug-eluting stent restenosis: an uncommon yet pervasive problem. Circulation. 2010;122:5–7.
3. Shirota T, Yasui H, Shimokawa H, Matsuda T. Fabrication of endothelial progenitor cell (EPC)-seeded intravascular stent devices and in vitro endothelialization on hybrid vascular tissue. Biomaterials. 2003;24:2295–302.
4. Stefanadis C, Toutouzas K, Tsiamis E, Vlachopoulos C, Kallikazaros I, Stratos C, *et al.* Stents covered by autologous venous grafts: feasibility and immediate and long-term results. Am Heart J. 2000;139:437–45.
5. Farhatnia Y, Tan A, Motiwala A, Cousins BG, Seifalian AM. Evolution of covered stents in the contemporary era: clinical application, materials and manufacturing strategies using nanotechnology. Biotechnol Adv. 2013;31:524–42.
6. Oh B, Lee CH. Nanofiber for cardiovascular tissue engineering. Expert Opin Drug Deliv. 2013;10:1565–82.
7. Chatterjea D, Wetzel A, Mack M, Engblom C, Allen J, Mora-Solano C, *et al.* Mast cell degranulation mediates compound 48/80-induced hyperalgesia in mice. Biochem Biophys Res Commun. 2012;425:237–43.
8. Levick SP, McLarty JL, Murray DB, Freeman RM, Carver WE, Brower GL. Cardiac mast cells mediate left ventricular fibrosis in the hypertensive rat heart. Hypertension. 2009;53:1041–7.
9. Tahara K, Tadokoro S, Yamamoto H, Kawashima Y, Hirashima N. The suppression of IgE-mediated histamine release from mast cells following exocytic exclusion of biodegradable polymeric nanoparticles. Biomaterials. 2012;33:343–51.
10. Xu JM, Shi GP. Emerging role of mast cells and macrophages in cardiovascular and metabolic diseases. Endocr Rev. 2012;33:71–108.
11. Botand I, Biessen EA. Mast cells in atherosclerosis. Thromb Haemost. 2011;106:820–6.

12. Lebduska P, Korb J, Tumova M, Heneberg P, Draber P. Topography of signaling molecules as detected by electron microscopy on plasma membrane sheets isolated from non-adherent mast cells. J Immunol Methods. 2007;328:139–51.
13. Brieger K, Schiavone S, Miller Jr FJ, Krause KH. Reactive oxygen species: from health to disease. Swiss Med Wkly. 2012;142:w13659.
14. Kirkinezos IG, Moraes CT. Reactive oxygen species and mitochondrial diseases. Semin Cell Dev Biol. 2001;12:449–57.
15. Swindleand EJ, Metcalfe DD. The role of reactive oxygen species and nitric oxide in mast cell-dependent inflammatory processes. Immunol Rev. 2007;217:186–205.
16. Hulsmans M, Van Dooren E, Holvoet P. Mitochondrial reactive oxygen species and risk of atherosclerosis. Curr Atheroscler Rep. 2012;14:264–76.
17. Irani K. Oxidant signaling in vascular cell growth, death, and survival: a review of the roles of reactive oxygen species in smooth muscle and endothelial cell mitogenic and apoptotic signaling. Circ Res. 2000;87:179–83.
18. Forstermann U, Munzel T. Endothelial nitric oxide synthase in vascular disease: from marvel to menace. Circulation. 2006;113:1708–14.
19. Yoo JW, Acharya G, Lee CH. In vivo evaluation of vaginal films for mucosal delivery of nitric oxide. Biomaterials. 2009;30:3978–85.
20. Koranteng RD, Dearman RJ, Kimber I, Coleman JW. Phenotypic variation in mast cell responsiveness to the inhibitory action of nitric oxide. Inflamm Res. 2000;49:240–6.
21. Iikura M, Takaishi T, Hirai K, Yamada H, Iida M, Koshino T, *et al.* Exogenous nitric oxide regulates the degranulation of human basophils and rat peritoneal mast cells. Int Arch Allergy Immunol. 1998;115:129–36.
22. Eastmond NC, Banks EM, Coleman JW. Nitric oxide inhibits IgE-mediated degranulation of mast cells and is the principal intermediate in IFN-gamma-induced suppression of exocytosis. J Immunol. 1997;159:1444–50.
23. Yip K, Leung F, Huang Y, Lau H. Inhibition of anti-IgE mediated human mast cell activation by NO donors is dependent on their NO release kinetics. Br J Pharmacol. 2009;156:1279–86.
24. Davis BJ, Flanagan BF, Gilfillan AM, Metcalfe DD, Coleman JW. Nitric oxide inhibits IgE-dependent cytokine production and Fos and Jun activation in mast cells. J Immunol. 2004;173:6914–20.
25. Alef MJ, Tzeng E, Zuckerbraun BS. Nitric oxide and nitrite-based therapeutic opportunities in intimal hyperplasia. Nitric Oxide. 2012;26:285–94.
26. Acharya G, Lee CH, Lee Y. Optimization of cardiovascular stent against restenosis: factorial design-based statistical analysis of polymer coating conditions. PLoS One. 2012;7:e43100. United States.
27. Oh B, Lee CH. Advanced cardiovascular stent coated with nanofiber. Mol Pharm. 2013;10:4432–42.
28. Xu C, Wang Y. Cross-linked demineralized dentin maintains its mechanical stability when challenged by bacterial collagenase. J Biomed Mater Res B Appl Biomater. 2011;96:242–8.
29. Yoo JW, Lee JS, Lee CH. Characterization of nitric oxide-releasing microparticles for the mucosal delivery. J Biomed Mater Res A. 2010;92:1233–43.
30. Yoo JW, Giri N, Lee CH. pH-sensitive Eudragit nanoparticles for mucosal drug delivery. Int J Pharm. 2011;403:262–7.
31. Mokudai T, Nakamura K, Kanno T, Niwano Y. Presence of hydrogen peroxide, a source of hydroxyl radicals, in acid electrolyzed water. PLOS ONE. 2012;7:e46392.
32. Yunos DM, Ahmad Z, Salih V, Boccaccini AR. Stratified scaffolds for osteochondral tissue engineering applications: electrospun PDLLA nanofibre coated Bioglass(R)-derived foams. J Biomater Appl. 2013;27:537–51.
33. Acharya G, Hopkins RA, Lee CH. Advanced polymeric matrix for valvular complications. J Biomed Mater Res A. 2012;100:1151–9.
34. Bhattarai N, Li Z, Edmondson D, Zhang M. Alginate-based nanofibrous scaffolds: structural, mechanical, and biological properties. Adv Mater. 2006;18:1463–7.
35. Bhattarai M, Zhang M. Controlled synthesis and structural stability of alginate-based nanofibers. Nanotechnology. 2007;18:455601.
36. Noor JI, Ikeda T, Ueda Y, Ikenoue T. A free radical scavenger, edaravone, inhibits lipid peroxidation and the production of nitric oxide in hypoxic-ischemic brain damage of neonatal rats. Am J Obstet Gynecol. 2005;193:1703–8.
37. Nakagawa H, Ohyama R, Kimata A, Suzuki T, Miyata N. Hydroxyl radical scavenging by edaravone derivatives: efficient scavenging by 3-methyl-1-(pyridin-2-yl)-5-pyrazolone with an intramolecular base. Bioorg Med Chem Lett. 2006;16:5939–42.
38. Suzuki Y, Yoshimaru T, Inoue T, Ra C. Discrete generations of intracellular hydrogen peroxide and superoxide in antigen-stimulated mast cells: reciprocal regulation of store-operated Ca2+ channel activity. Mol Immunol. 2009;46:2200–9.
39. Aggarwal BB, Harikumar KB. Potential therapeutic effects of curcumin, the anti-inflammatory agent, against neurodegenerative, cardiovascular, pulmonary, metabolic, autoimmune and neoplastic diseases. Int J Biochem Cell Biol. 2009;41:40–59.
40. Curzonand G, Green AR. Rapid method for the determination of 5-hydroxytryptamine and 5-hydroxyindoleacetic acid in small regions of rat brain. Br J Pharmacol. 1970;39:653–5.
41. Dearman RJ, Skinner RA, Deakin N, Shaw D, Kimber I. Evaluation of an in vitro method for the measurement of specific IgE antibody responses: the rat basophilic leukemia (RBL) cell assay. Toxicology. 2005;206:195–205.
42. Suzuki Y, Yoshimaru T, Yamashita K, Matsui T, Yamaki M, Shimizu K. Exposure of RBL-2H3 mast cells to Ag(+) induces cell degranulation and mediator release. Biochem Biophys Res Commun. 2001;283:707–14.
43. Sun J, Sukhova GK, Wolters PJ, Yang M, Kitamoto S, Libby P, *et al.* Mast cells promote atherosclerosis by releasing proinflammatory cytokines. Nat Med. 2007;13:719–24.
44. Swindle EJ, Metcalfe DD, Coleman JW. Rodent and human mast cells produce functionally significant intracellular reactive oxygen species but not nitric oxide. J Biol Chem. 2004;279:48751–9.